Original Research Article

Manta-Ray-Inspired Bump Geometry for Enhanced Mixing in a Straight Microchannel

Serah Yang

Providence Christian Academy, Seoul, 05510, Republic of Korea

ABSTRACT

Slow diffusion in laminar microchannels limits assay speed, so a simple passive way to enhance mixing isuseful. This study tests whether smooth, periodic wall bumps inspired by manta rays can outperform astraight Y-junction of the same footprint. Both geometries were built, 3D computational fluid dynamics(CFD) was conducted in Ansys Student 2025 R2 with laminar flow and species transport, and mixing wascompared at inlet flow ratios of 1:1, 1:2, and 1:3 for water with dilute fluorescein. The bumped channelshowed earlier and broader regions of intermediate concentration and a more uniform outlet profile acrossall ratios, with a higher but manageable pressure drop. Velocity maps were consistent with low Reynoldsnumber flow, while pressure fields showed small local rises before bumps and dips after them. Mesh sizeand solver settings may soften gradients near bumps, but trends were consistent. These results supportfabrication and testing of the bumped design for low-flow lab-on-a-chip applications that need bettermixingwithoutaddedhardware.

Keywords: Microfluidics; laminar mixing; passive micromixer; biomimicry; CFD; PDMS; species transport

INTRODUCTION

At sub-millimeter scales, Reynolds numbers are low, and two streams mostly mix by diffusion, which cantake centimeters. Passive micromixers use fixed geometry to stretch and fold interfaces so diffusion acts over shorter distances. Ray gill textures suggest useful motifs for controlled vortices and interfacial renewal. It was asked if smooth, periodic wall bumps inspired by manta rays would improve mixing in a straight channel compared to a plain Y-junction with the same footprint.

Living organisms move liquids with efficiency that still challenges engineered systems. Tree vessels liftsap through small channels, spider silk condenses fog into droplets, and fish gills sweep large volumes ofwater. By taking inspiration from these systems, biomimicry has yielded water-shedding coatings and underwater adhesives. Nature is a useful design guide for microfluidics because many biological channel sizes mirror those used on chips (1, 2).

Microfluidics took shape in the early 1990s as researchers etched micrometer-scale channels in silicon and glass using UV photolithography borrowed from semiconductor processing. The advent of soft lithography with poly(dimethylsiloxane) (PDMS) enabled rapid, low-costprototyping: a master is patterned, PDMS is cast and cured, then bonded to glass to form sealed channels. PDMS offers opticalclarity, easy bonding, chemical compatibility with many aqueous samples, and gas

Corresponding author: Serah Yang, E-mail: sarah1006y@gmail.com.

Accepted January 31, 2026
https://doi.org/10.70251/HYJR2348.41581591

permeability that supports cell culture, which helped labs move from concept to experiment in hours rather than days (3, 4).

At sub-millimeter scales, Reynolds numbers are typically below one, so flows are laminar, and two streams mix mainly by diffusion. Complete mixing can require centimeter-scale distances, which is too long for time-critical assays (1, 2). Micromixers address this in two ways. Passive designs embed fixed features, such as serpentine bends or staggered herringbones, that stretch and fold interfaces to accelerate diffusion (5). Recent studies in 2023 and 2024 have further refined these passive structures, utilizing Norman windows and optimized split-and-recombine layouts to enhance mixing at low Reynolds numbers (6, 7). Active designs impose acoustic, electric, or thermal fields to stir the flow, but they add hardware and can perturb sensitive samples (2).

Biologically inspired textures provide another route. Rows of lobes and bumps on ray gill structures generate paired vortices that manage particles without clogging, suggesting motifs that might enhance mixing in channels. A recent 2024 study of mobula rays quantified a permeability-selectivity trade-off via a leaky-channel model that links flow rate, plate spacing, and vortex formation (8). A PDMS microfilter patterned with manta-inspired ribs formed controlled vortices that redirected particles while resisting fouling, offering practical guidance on rib spacing and operating flow (9). In parallel, geometric refinements in passive mixers have shown strong gains: shallow cavities and recessed steps can host stable Dean-type rolls and reduce pressure demand, while split-and-recombine layouts fold interfaces repeatedly to drive composition toward uniformity with low loss (10, 11). Under moderate laminar conditions, groove-based designs can reach near-complete mixing on millisecond time scales at microliter-per-minute rates (12).

In this study, it was aimed to evaluate how smooth, periodic wall bumps inspired by manta rays could be used as a potential design feature for a micromixer. Through the use of computational fluid dynamics (CFD) simulations, the mixing behavior of this channel was compared with a control Y-junction smooth channel. The study looks at the behavior of these channels across a range of flow velocities and at three different flow ratios. This study aims to evaluate whether manta-ray-inspired wall bumps can enhance mixing efficiency compared with a Y-junction control under laminar flow conditions using 3D CFD simulations.

METHODSANDMATERIALS

Device design and geometry

Two micromixer geometries were modeled using OnShape: a Y-junction control and a manta-ray-inspired channel with wall bumps. Each device has a straight rectangular main channel that is 0.5 mm wide and 27.983 mm long, with 9.058 mm from inlet to center and 18.925 mm from center to outlet. For the manta-ray design, bumps are integrated along the main channel walls with a streamwise spacing of 1 mm, an angle of 49.251°, and a maximum protrusion depth of 0.09412 mm measured from the nominal wall toward the channel interior. The Y-junction control has the same footprint but no internal features after the merge.

Computational setup and solver

All simulations were three-dimensional and performed in Ansys Student 2025 R2. The laminar flow model and the species transport model were used.The working fluid was water carrying a dilute fluorescein dye; the dye was treated as a passive scalar with constant molecular diffusivity $D = 4.25 \times 10^{-10}$ m^2 s^{-1}. Fluid properties were assumed incompressible, Newtonian, and isothermal.

Boundary and initial conditions

Each device used two inlets and one outlet. Inlet velocities were prescribed to set the desired flow conditions. The primary test cases used an inlet bulk speed of 0.001 m s^{-1} and three inlet flow ratios: 1:1, 1:2, and 1:3. The operating range considered for sensitivity was 0.001 to 0.003 m s^{-1}. Species boundary conditions were set as $c = 1$ at the dyed inlet and $c = 0$ at the water inlet. The outlet was a pressure outlet at 0 Pa gauge. A no-slip condition was applied on all solid walls.

Meshing

Both geometries were discretized with unstructured tetrahedral elements at a nominal size of 0.1 mm. The same base size was used for the Y-junction control and the manta-ray channel. Local resolution increases naturally around the bumps due to curvature and narrow passages, but no separate sizing smaller than 0.1 mm was imposed.

Solver controls

The steady laminar flow solution was obtained first, followed by the steady species field on the same mesh. Step size and iterations per step followed the project

spreadsheet. Computational constraints necessitated use of a reduced iteration count for manta-ray cases than the Y-junction control. This choice and its implications fornumerical diffusion and gradient sharpness are discussed in the Discussion section.

Outputs and post-processing

Velocity magnitude, static pressure, and dye concentration contours were exported along the channel center plane and at selected cross-sections. For mixing, concentration maps were examined qualitatively, and outlet cross-section profiles were extracted for comparison between devices and flow ratios. Total pressure drop between inlet and outlet planes was recorded for each case.

RESULTS

Overviewandrationale.

A manta-ray-inspired micromixer was compared to a Y-junction control with the same footprint to test whether internal bumps improve mixing in a straight, laminar microchannel. Each device was modeled in 3D and solved in Ansys Student 2025 R2 using laminar flow and specie stransport.

Overview of micromixer geometry

The Y-junction (Figure 1a) consisted of a straight rectangular channel with no internal features; dimensions are detailed in Table 1. The manta-ray channel (Figure 1b) used the same cross-section and length as the Y-junction but introduced periodic bumps that narrowed and widened the passage locally.

Velocity and pressure distribution at 1:1

In order to establish baseline hydrodynamics before comparing mixing, laminar flow was solved to steady state. Subsequently, velocity magnitude and static

Table 1. Dimensions of Y-junction and manta ray channels.

Parameter	Y-junction channel	Manta ray channel
Width	0.5 mm	0.5 mm
Length	27.983 mm	27.983 mm
Depth	50 µm	50 µm
Other parameters	N/A	Bump spacing = 1 mm Bump angle = 49.251° Bump depth = 0.09412 mm

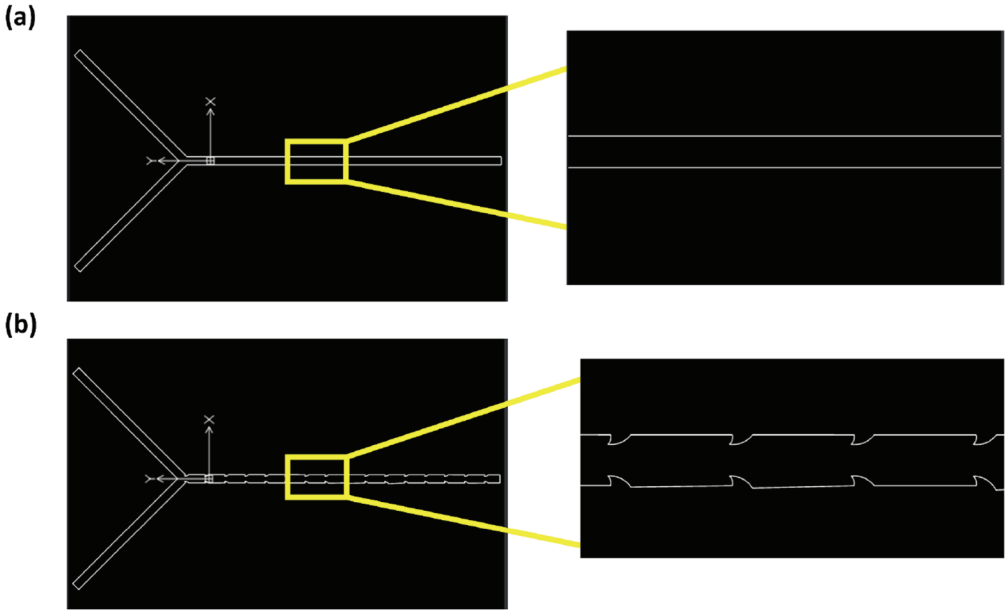

Figure 1. ***CAD drawings of Y-junction and manta ray channels.*** *(a) (Left) Drawing showing geometry of Y-junction channel, (Right) Zoomed-in image of channel to emphasize absence of features. (b) Drawing showing geometry of manta ray channel, (Right) Zoomed-in image of channel to show presence of bumps in channel.*

pressure fields were exported along the mid-plane and at cross-sections. Across all six runs, velocity-magnitude contours appeared uniformly blue on the chosen legend, indicating very low speeds at the operating Reynolds numbers (Figure 2). No higher-speed core was evident in the Y-junction, and local accelerations around bumps were not resolved in the manta-ray channel on this scale. Pressure fields still distinguished the designs at 1:1. The Y-junction showed a smooth axial decline consistent with laminar duct flow (Figure 3a), while the manta-ray mixer required a higher overall pressure drop and showed small local rises just upstream of bumps with dips just downstream, superimposed on the global decline (Figure 3b). Pressure drop increased by ~20% in the manta-ray channel compared with control. The inlet-to-outlet pressure drop values for each case are reported in Table 2 and should be taken into consideration when evaluating pumping requirements.

Comparison of mixing efficiency at 1:1 flow ratio

To test whether bumps improve mixing under symmetric inflow, a passive scalar c was injected with c = 1 at the dyed inlet and c = 0 at the water inlet; the steady species field was computed on the

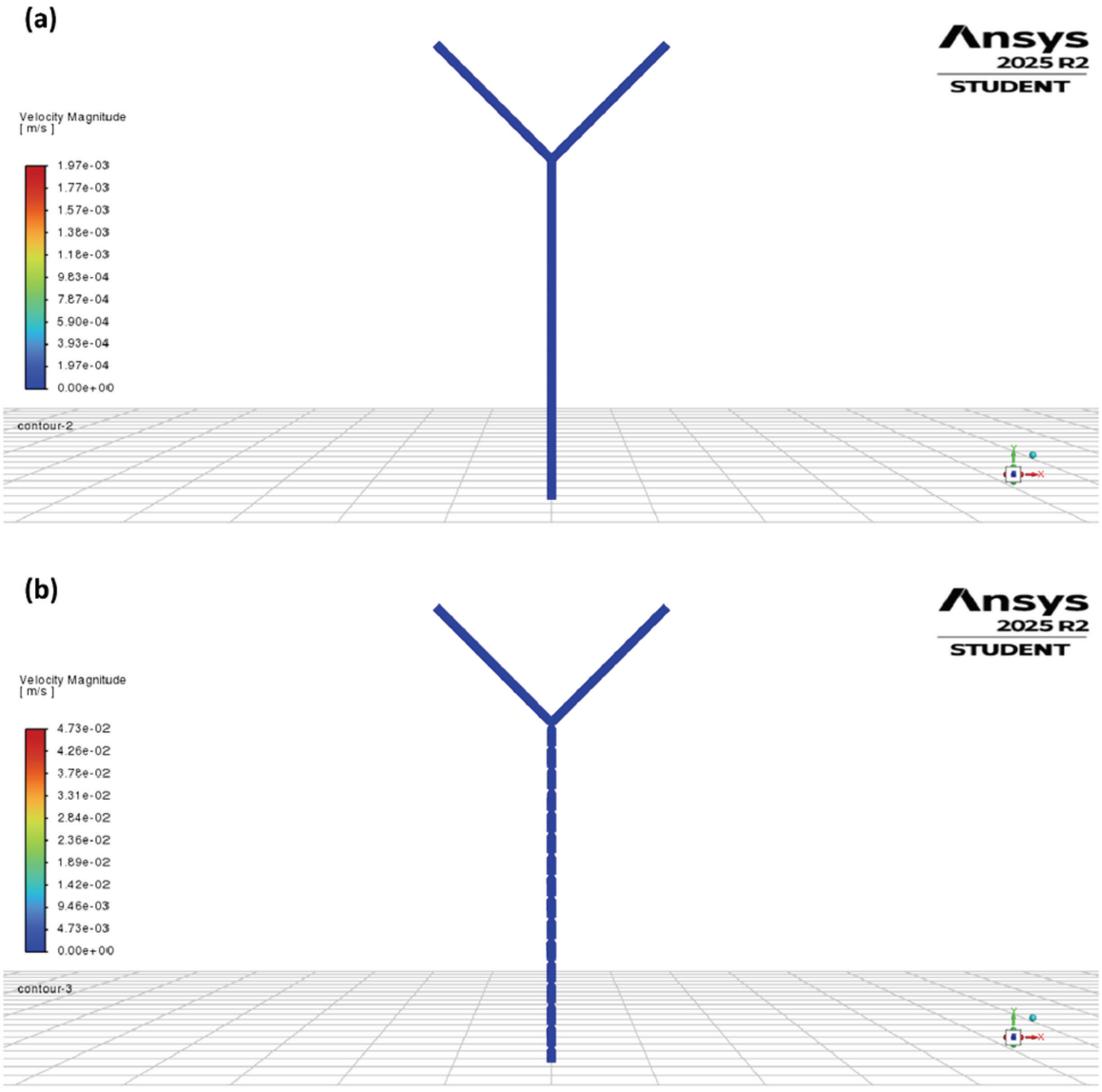

Figure 2. ***Flow velocity profiles of Y-junction and manta ray channels at 1:1 flow ratio.*** *(a) Velocity profile of Y-junction channel. (b) Velocity profile of manta ray channel.*

Table 2. Pressure data across the Y-junction and manta ray channels.

Type ofchannel	Flow ratio	Water inlet pressure(Pa)	Water + dye inletpressure (Pa)	Outlet pressure (Pa)
Y-junction	1:1	2.143	2.135	0
	1:2	3.065	3.476	0
	1:3	4.009	4.854	0
Manta ray	1:1	2.545	2.541	0
	1:2	4.109	3.657	0
	1:3	5.737	4.851	0

Note: The extracted data was rounded to 3 decimal places.

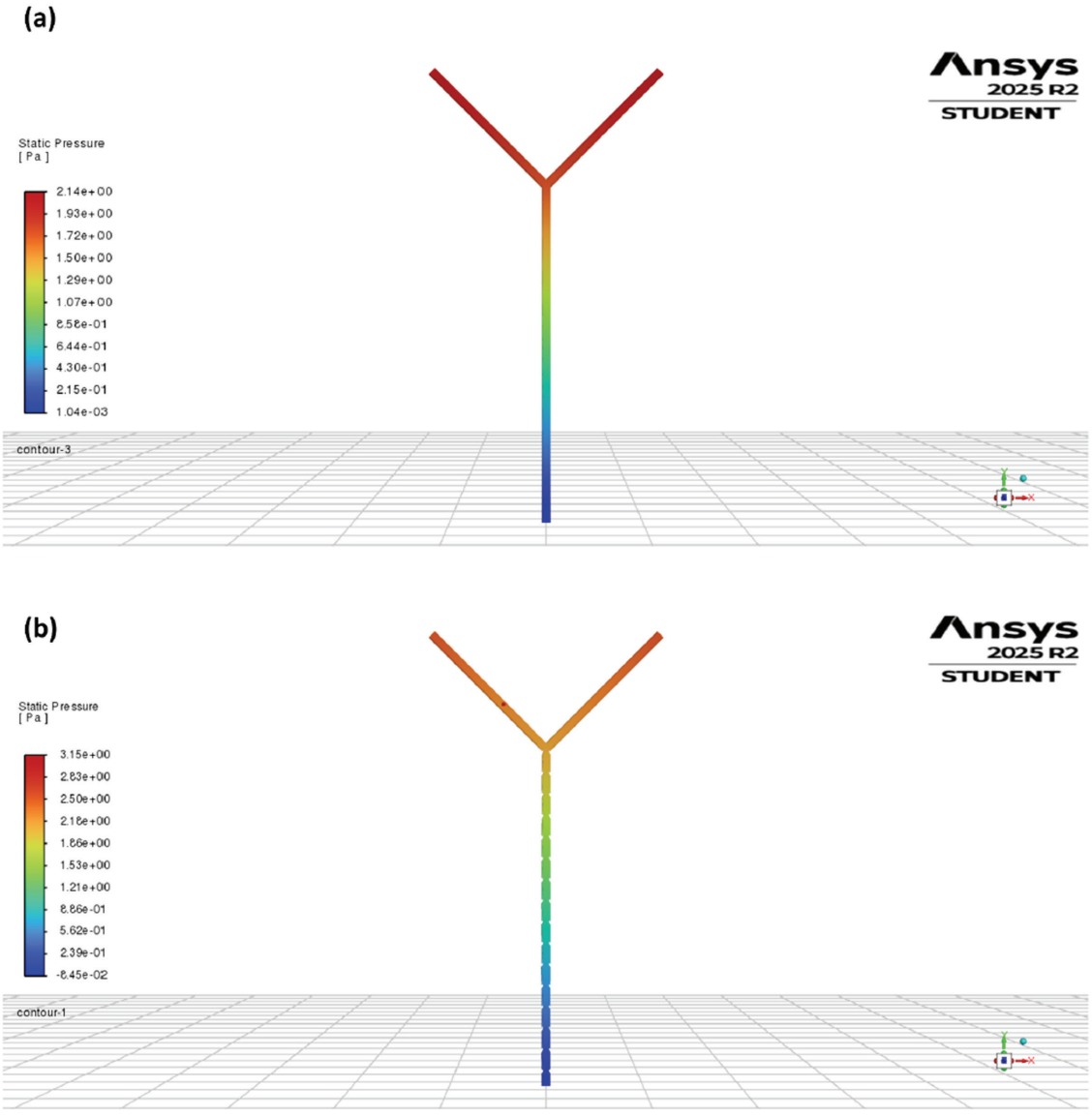

Figure 3. ***Profiles showing variation in pressure across Y-junction and manta ray channels at 1:1 flow ratio.*** *(a) Variation in pressure across the Y-junction channel. (b) Variation in pressure across the manta ray channel.*

converged flow. Concentration maps and outlet cross-section profiles were extracted. In the Y-junction, two layered streams remained with a thin diffusive band that widened slowly downstream; red and blue regions persisted at the outlet with a middle band of green-yellow (Figure 4a). In the manta-ray mixer, repeated interface deformation produced earlier and broader regions of intermediate concentration and a more uniform outlet profile (Figure 4b).

Mixing at unequal flow ratios, 1:2 and 1:3

In order to assess robustness when one inlet dominates the flow, the inlet velocity ratio was set to 1:2 and 1:3 while holding total flow fixed at 0.001 m s^{-1} per inlet stream in the base case; steady concentration fields and outlet profiles were extracted. In the Y-junction, the dominant stream occupied a larger fraction of the cross-section, pushing the minority stream to the wall and leaving large unmixed regions at the outlet for both 1:2 and 1:3 (Figure 5a, Figure 6a). In the manta-ray mixer, the bumps continued to fold the minority stream into the bulk, producing broader regions of intermediate concentration and a smoother outlet profile, though the advantage narrowed at 1:3 compared with 1:1 (Figure 5b, Figure 6b).

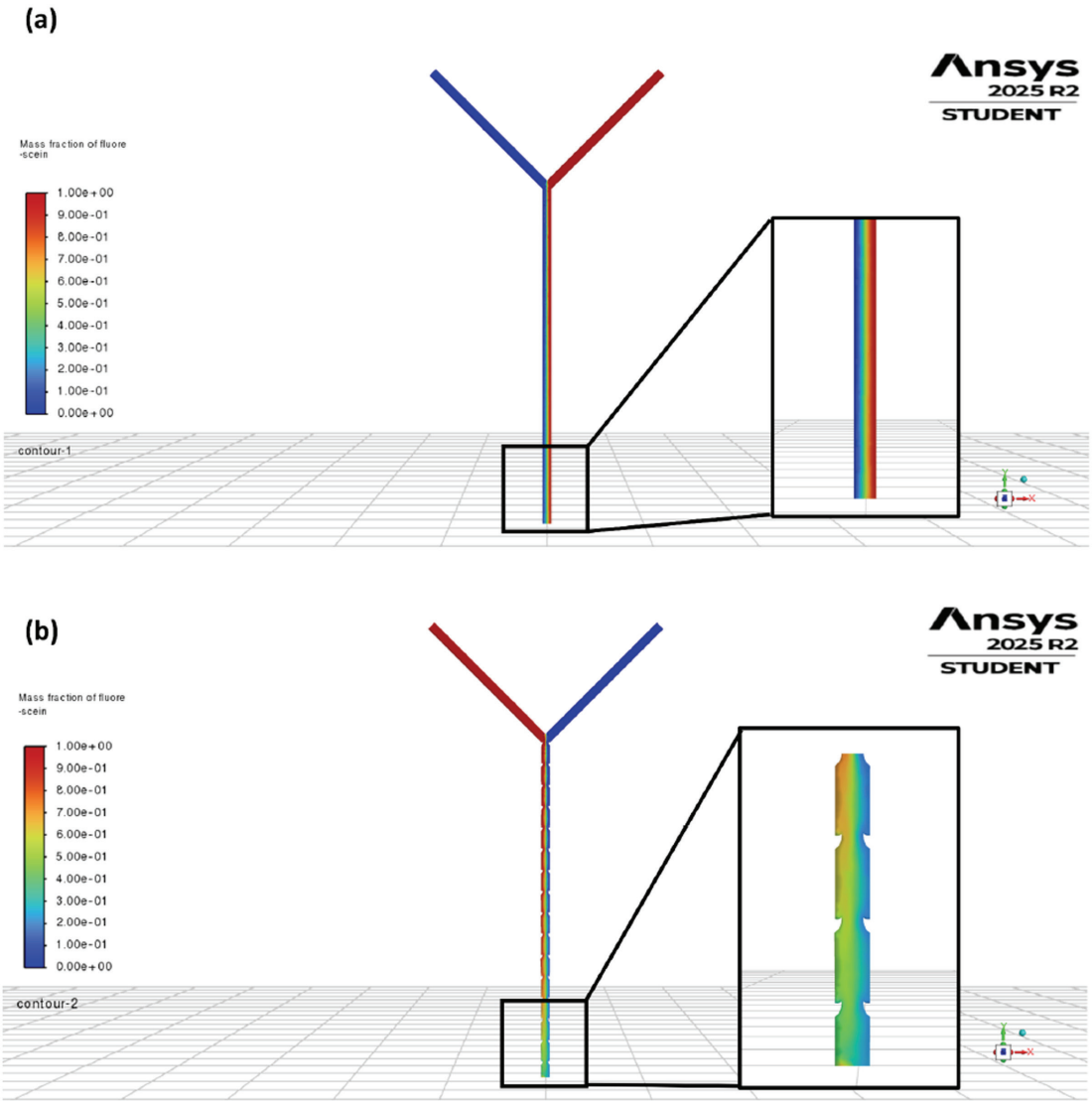

Figure 4. Profiles showing mixing behaviour in Y-junction and manta ray channels at 1:1 flow ratio. *(a) Mixing behaviour in the Y-junction channel, (inset) zoomed-in image of mixing behaviour at the channel outlet. (b) Mixing behaviour in the manta ray channel, (inset) zoomed-in image of mixing behaviour at the channel outlet.*

Notes on numerical settings relevant to interpretation (Table S1).

It is important to note that CFD solver settings could influence gradients. Therefore, time step and iteration counts were logged for each case. Due to computational constraints necessitated by the system on which the simulations were carried out, the manta-ray cases used larger time steps and fewer iterations than the Y-junction. This can introduce numerical diffusion and slightly soften concentration gradients, so gradient-sensitive values in Table S1 should be interpreted with this context in mind. Mesh size was 0.1 mm tetrahedra for both devices; the settings used per run are summarized in Table S1.

Figure and table references

Figure 1, device geometry; Figure 2, velocity magnitude; Figure 3, static pressure; Figure 4, concentration at 1:1; Figures 5–6, concentration at 1:2 and 1:3; Table 1, geometry parameters; Table 2, pressure drops; Table S1, solver controls.

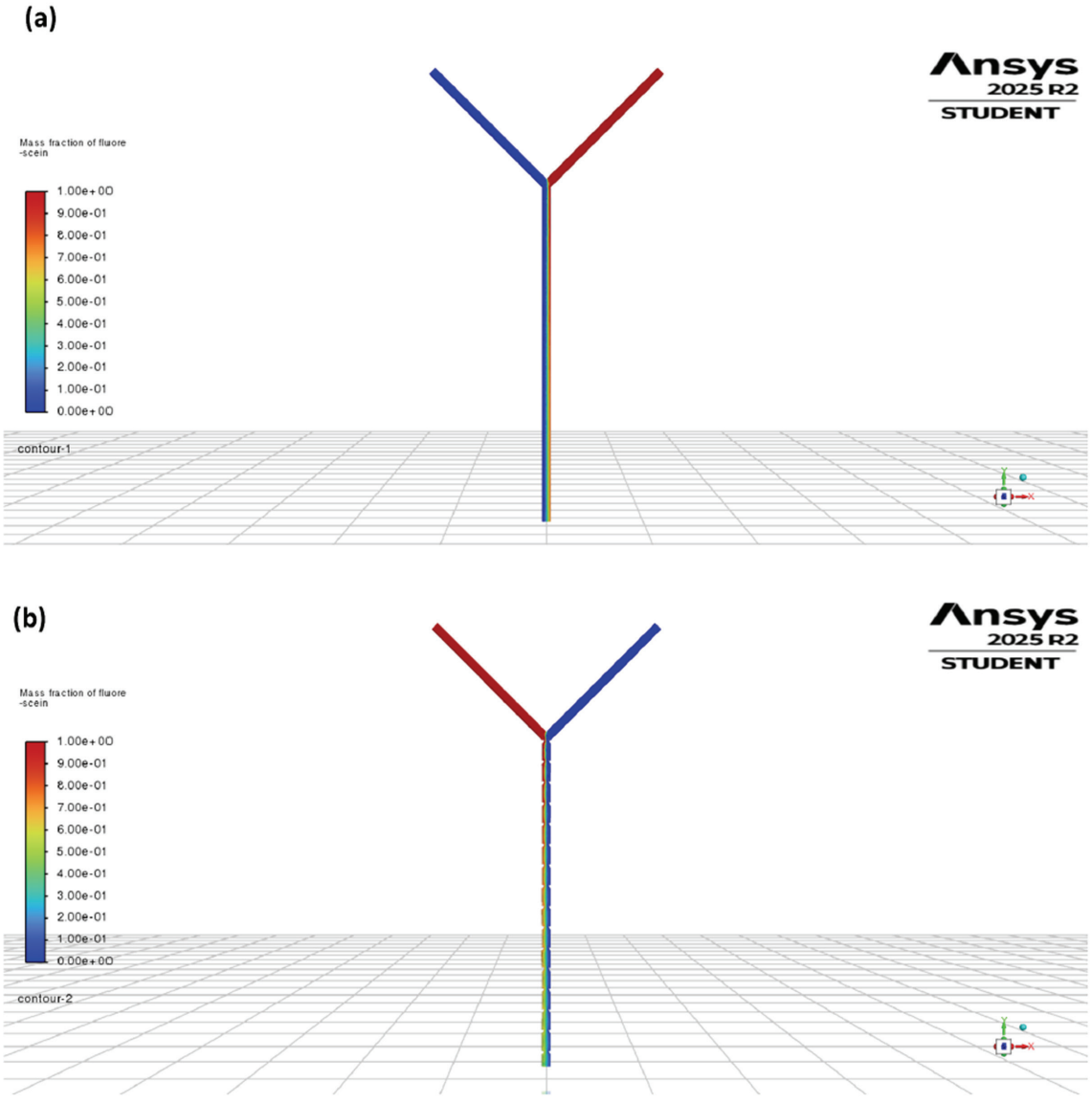

Figure 5. Profiles showing mixing behaviour in Y-junction and manta ray channels at 1:2 flow ratio. *(a) Mixing behaviour in the Y-junction channel (b) Mixing behaviour in the manta ray channel.*

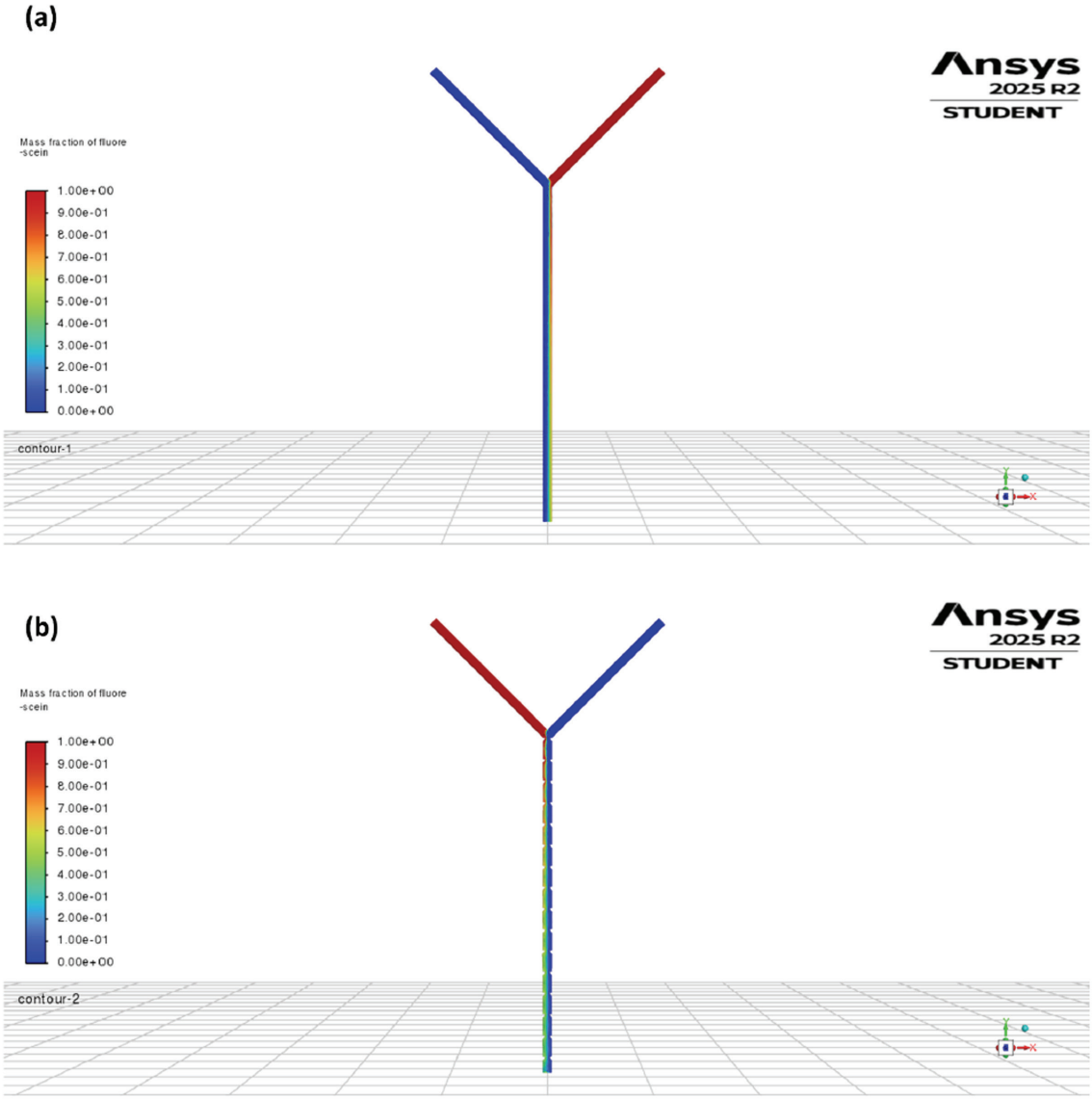

Figure 6. ***Profiles showing mixing behaviour in Y-junction and manta ray channels at 1:3 flow ratio.*** *(a) Mixing behaviour in the Y-junction channel. (b) Mixing behaviour in the manta ray channel.*

Table S1. CFD solver controls.

Type ofchannel	Mesh size (mm)	Time step size (s)	Number of iterations per step	Total simulationtime (s)
Y-junction	0.1	0.1	20	20
Manta ray	0.1	0.5	5	20

DISCUSSION

The simulations showed that the manta-ray micromixer outperformed the Y-junction control for mixing while requiring a higher, still manageable, pressure drop. At 1:1, the control retained two layered streams with only a thin diffusive band at the interface, whereas the manta-ray channel produced earlier and broader regions of intermediate concentration and a more uniform outlet profile (Figure 4). Under unequal inlet flow ratios, 1:2 and 1:3, the control pushed the minority stream against a wall and left large unmixed regions, while the manta-ray design continued to fold the minority stream into the bulk and maintained wider mixed zones, though the advantage narrowed at 1:3 (Figures 5–6). Velocity maps appeared uniformly low on the chosen scale across all runs, consistent with the low Reynolds number regime, yet the pressure fields distinguished the designs: the manta-ray channel showed a higher total drop with small local rises ahead of bumps and dips downstream, superimposed on the global decline seen in the control (Figure 3, Table 2). Together these observations support the hypothesis that smooth periodic bumps increase interfacial area and induce mild transverse motion, improving mixing relative to a straight Y-junction of the same footprint, at a modest cost in pressure (approximately 20% increase over the control). This interpretation is consistent with known laminar mixing mechanisms in microchannels, where stretching and folding of interfaces accelerate diffusion without turbulence (1, 2, 5).

Several factors could have influenced the outcomes. First, the bumped geometry is harder to resolve than the plain channel. Computational constraints necessitated use of a reduced iteration count for manta-ray cases than the control, which can add numerical diffusion and soften gradients near the bumps. Steady outlet concentration and pressure were reported and conservation was checked, but some under-resolution of sharp interfaces is possible. Second, both devices were meshed with 0.1 mm tetrahedra. While this base size matched across cases, local refinement along walls and in the narrow passages around bumps would better capture near-wall shear and cross-stream transport. A standard remedy is to run a mesh-independence study with targeted refinement and tighter convergence tolerances, which is identified as future work. Third, the velocity color scale compressed small variations at low speeds, which explains the uniformly blue magnitude maps. The pressure plots still captured design differences, but future figures should include scaled velocity slices or streamline plots to better show secondary motion if present. These limitations do not overturn the main comparisons, but they add uncertainty to gradient-sensitive quantities and should be addressed before design lock.

The choice of test matrix also shaped the conclusions. It was compared 1:1, 1:2, and 1:3 at an inlet speed of 0.001 m s^{-1}, which is a relevant flow velocity for microfluidics. Additional points in velocity and geometry space would help map the trade between mixing and pressure drop. In particular, sweeping bump height, angle, and spacing can reveal whether there is a broad optimum or a narrow peak. Extending the module count would show whether mixing gains compound linearly or saturate with length, an outcome often seen in passive mixers that rely on repeated stretching cycles (5). It would also be informative to test a short pulsed or oscillatory inlet to see if mild unsteadiness further enhances interfacial renewal in this geometry without adding hardware.

The significance of these results is practical. Many microfluidic assays need better mixing than a straight Y-junction can provide but cannot tolerate bulky actuators or high pressure penalties. Portable and point-of-care chips must stay small and low power, so external pumps or actuators add footprint, cost, and setup time. High pressures can distort channels and increase the chance of leaks and bond failure, particularly in PDMS. Additionally, they increase shear, which can dissolve surface coatings, denature proteins, or harm cells. Since microliter samples are used in many assays, increased pressure results in longer runs or higher consumption. These limitation sencourage low-pressure passive mixing. The manta-ray bumps are easy to define in CAD, fit in the same footprint, and improved outlet uniformity across equal and unequal inlets in our simulations. This makes the design a plausible candidate for lab-on-a-chip devices that run at low flow rates and small volumes, where passive structures are preferred over active fields. Generality is not claimed beyond the tested conditions. The data support the hypothesis for the geometries and flow settings studied. They do not prove that all manta-like patterns will outperform every passive alternative, nor do they establish behavior at much higher Re or with non-Newtonian samples. Correlation between bumps and improved mixing in our CFD does not imply causation in every context without experimental confirmation.

Future work should address both computation and experiment. On the computation side, a mesh-independence study is planned with local refinement over each bump, inflation layers at walls, and tighter residual

targets, plus a small parameter sweep of bump height, angle, and spacing. On the experimental side, a PDMS device made from a high-resolution master would allow validation with water and fluorescein under syringe-pump control. Imaging along the channel can quantify concentration fields and a mixing index at matched flow ratios, and inline sensors or calibrated pump pressures can provide pressure drop data. It could also be employed spectroscopic evaluation of the fluid collected from the outlet to determine the level of mixing that has occurred in the channel. Tests with particle-laden samples can check for bubble trapping or fouling in recirculation pockets, which matters for real samples. If confirmed, the geometry can then be tuned to hit target mixing at acceptable pumping power for specific applications. Examples include mixing swab eluate or saliva with lysis buffer for PCR or CRISPR tests, pre-mixing blood or plasma with reagents for bead-based immunoassays, small-volume enzyme assays where the color signal depends on uniform contact, and on-chip dilution series for antibiotic susceptibility tests. Stable operation over several runs, minimal bubble trapping, and consistent outlet concentration at the tested flow ratios would be success criteria.

In summary, the manta-ray-inspired channel mixed more effectively than an equal-footprint Y-junction in 3D CFD, with earlier and broader intermediate concentration regions at 1:1 and a retained advantage at 1:2 and 1:3, balanced by a higher total pressure drop. Limits on mesh resolution and iteration counts may have softened gradients near bumps, but the design-level trends were consistent with laminar mixing theory and with the pressure behavior expected in repeated contraction–expansion paths (1, 2, 11). The findings suggest a simple passive path to better mixing in straight microchannels and motivate fabrication and targeted optimization rather than wholesale changes to device architecture.

CONCLUSION

The manta-inspired bumped channel improved mixing across 1:1, 1:2, and 1:3 inlet ratios in steady CFD relative to a same-footprint Y-junction, with a manageable pressure penalty. However, this study is limited by the computational constraints that necessitated reduced iteration counts for the bumped geometry, potentially introducing numerical diffusion that could soften sharp concentration gradients. Mesh resolution was also limited by a uniform 0.1 mm tetrahedron size. Future work should focus on a mesh-independence study with local refinement and experimental validation using PDMS devices to confirm that observed design-level trends translate to physical applications. These findings suggest a simple passive path to better mixing in straight microchannels and motivate fabrication and targeted optimization.

ACKNOWLEDGEMENTS

The author thanks Dr. Kadgathur Jayaram for guidance on study design and feedback on the CFD setup. The author also thanks Mr. Joon and Mr. Tophy, teachers at Providence Christian Academy Korea, for comments on early drafts and their support. This work used Onshape Education and Ansys Student licenses. Any errors are theauthor's own.

FUNDING SOURCES

The author received no specific funding for this work.

CONFLICT OF INTEREST

The author declares no conflicts of interest.

REFERENCES

1. Stone HA, Stroock AD, Ajdari A. Engineering flows in small devices: microfluidics toward a lab-on-a-chip. *AnnuRev Fluid Mech.* 2004; 36: 381-411. https://doi.org/10.1146/annurev.fluid.36.050802.122124
2. Squires TM, Quake SR. Microfluidics: fluid physics at the nanoliter scale. *Rev Mod Phys*. 2005; 77 (3): 977-1026. https://doi.org/10.1103/RevModPhys.77.977
3. Convery NM, Gadegaard N. 30 years of microfluidics. *Lab Chip.* 2019; 19: 196-215. https://doi.org/10.1016/j.mne.2019.01.003
4. Xia Y, Whitesides GM. Soft lithography. *Angew Chem Int Ed.* 1998; 37 (5): 550-575. https://doi.org/10.1002/(SICI)1521-3773(19980316)37:5<550::AID-ANIE550>3.0.CO;2-G
5. Stroock AD, Dertinger SKW, Ajdari A, MezicI, Stone HA, Whitesides GM.Chaotic mixer for microchannels. *Science*. 2002; 295 (5555): 647-651. https://doi.org/10.1126/science.1066238
6. Juraeva D, *et al*. Design of a passive microfluidic vortex mixer with a Norman window and baffles for enhanced mixing efficiency and reduced pressure drop. *Micromachines*. 2023; 14 (5): 1078. https://doi.org/10.3390/mi14051078

7. Nishu B, Samad AA. A split-and-recombine micro-mixer for efficient mixing at low Reynolds numbers. *Heliyon*. 2023; 9 (5): e16028. https://doi.org/10.1016/j.heliyon.2023.e14745
8. Mao X, Bischofberger I, Hosoi AE. Permeability-selectivity trade-off for a universal leaky channel inspired by Mobula filters. *Proc Natl Acad Sci USA*. 2024; 121: e2410018121. https://doi.org/10.1073/pnas.2410018121
9. Clark BD, San-Miguel A. Inspiration from ceramics of manta rays to realizea self-cleaning microfluidic chip. *iScience*. 2021; 24 (7): 102814.
10. Liao Y, Mechulam Y, Lassalle-Kaiser B. A millisecond passive microfluidic mixer with low sample consumption. *SciRep.* 2021; 11: 24131. https://doi.org/10.1038/s41598-021-99471-x
11. White FM. Fluid Mechanics. 9th ed. McGraw-Hill; 2021.
12. Ferziger JH, Perić M. Computational Methods for Fluid Dynamics. 3rded. Springer; 2002. https://doi.org/10.1007/978-3-642-56026-2
13. ANSYS, Inc. Species Transport and Finite-Rate Chemistry. Fluent Theory Guide. Accessed [Oct7, 2025].